An Integrated Strategy towards Self-Powering and Selectivity Tuning of Semiconductor Gas Sensors

Alaaeldin Gad [a,b,e §], Martin W.G. Hoffmann [a, b,c §], Olga Casals [c §], leonhard Mayrhofer [f,g], Cristian Fàbrega [c], Lorenzo Caccamo [a,b], Francisco Hernández-Ramírez [c,d], Matin S. Mohajerani [a,b], Michael Moseler [f,g], Hao Shen [a], Andreas Waag [a,b], Joan D. Prades [c,*]

[a] Institute for Semiconductor Technology, Braunschweig University of Technology, Hans-Sommer-Straße 66, D-38106 Braunschweig, Germany

[b] Laboratory of Emerging Nanometrology LENA, Langer Kamp 6a, Braunschweig, Germany

[c] MIND-IN2UB, Department of Engineering Electronics, University of Barcelona, C/Martí i Franquès 1, E-08028 Barcelona, Spain

[d]Catalonia Institute for Energy Research (IREC), Jardins de les Dames de Negre 1, Sant Adrià del Besòs, E-08930 Barcelona, Spain

[e]Inorganic Chemistry Department, National Research Centre (NRC), Cairo, Egypt

[f]Fraunhofer Institute for Mechanics of Materials IWM, D-79108 , Freiburg , Germany

[g]Freiburg Materials Research Center, University of Freiburg, D-79104 Freiburg, Germany

KEYWORDS: Self-powered, selectivity, organic-inorganic hybrid nanostructures, conductometric gas sensor, heterostructures, self-assembled monolayers

ABSTRACT: Inorganic conductometric gas sensors struggle to overcome limitations in high power consumption and poor selectivity. Herein, recent advances in developing self-powered gas sensors with tunable selectivity are introduced. Alternative general approaches for powering gas sensors were realized via proper integration of complementary functionalities (namely; powering and sensing) in a singular heterostructure. These solar light driven gas sensors operating at room temperature without applying any additional external powering sources are comparatively discussed. The TYPE-1 gas sensor based on integration of pure inorganic interfaces (e.g. CdS/n-ZnO/p-Si) is capable of delivering a self-sustained sensing response, while it shows a non-selective interaction towards oxidizing and reducing gases. The structural and the optical merits of TYPE-1 sensor are investigated giving more insights into the role of light activation on the modulation of the self-powered sensing response. In the TYPE-2 sensor, the selectivity of inorganic materials is tailored through surface functionalization with self-assembled organic monolayers (SAMs). Such hybrid interfaces (e.g. SAMs/ZnO/p-Si) have specific surface interactions with target gases compared to the non-specific oxidation-reduction interactions governing the sensing mechanism of simple inorganic sensors. The theoretical modeling using density functional theory (DFT) has been used to simulate the sensing behavior of inorganic/organic/gas interfaces, revealing that the alignment of organic/gas frontier molecular orbitals with respect to the inorganic Fermi level is the key factor for tuning selectivity. These platforms open new avenues for developing advanced energy-neutral gas sensing devices and concepts.

Future environmental monitoring technologies require sensing devices with minimal powering needs and selective detection capabilities to enable their integration in mobile devices or in the newly emerging miniaturized electronics. Inorganic gas sensors (e.g. metal oxides, MOx) need an external power unit in order to provide two functions. First, to generate the sensor read out signal which is derived by applying a constant bias current and monitoring the resistance changes upon exposure of different gases. Second, to provide the activation energies necessary for the interaction of gas molecules with the oxide surface, since the gas adsorption or desorption on MOx is an endothermic processes [1]. Typically, thermal heating (in the range of 200-500 ˚C) or non-equilibrium processes (light illumination, UV or visible) are applied to provide the needed energies for surface activation [2,3]. Recently, we reported a promising concept to realize self-powered gas sensors that are capable of detecting gases at zero power. It is based on using a multifunctional singular heterostructure capable on one hand of harvesting solar light (to drive the sensing signal and to provide the needed activation energy) and on the other hand of providing good sensing properties [4]. In this regard, n-doped MOx (such as ZnO, SnO_2) are good candidates to fulfill such requirements as they can form p-n

junction solar cells with p-doped semiconductors (e.g. Si) (for light harvesting). Also, they are among the highly robust gas sensors that have been intensively studied in literature and are commonly used in commercial applications [4,5,6]. For example, in the TYPE-1 gas sensor that is based on pure inorganic semiconductor heterostructures (e.g. CdS/n-ZnO/p-Si), the self-powered mode of operation was achieved while showing the expected non-selective sensing behavior toward both oxidative and reducing gases. The details of the sensing mechanism were discussed in a previous report [4]. Here, the structural properties of the integrated sensing and powering units of this approach are investigated. Moreover, the optical properties are studied to reveal the key factors governing the self-powered sensing responses.

Besides the powering necessities, selectivity of inorganic semiconductors remains a challenging issue that needs to be addressed. As a result of their non-selective redox interaction with gas molecules, gas sensors based on pure inorganic metal oxides show poor selectivity [3]. Different bioinspired approaches have found their way into gas sensing application due to the appealing analogies of both fields [7,8]. High selectivity toward a single gas species can be achieved via the binding of the analyte gas with free organic functional groups anchored on the sensor surface. In this respect, modifying the inorganic semiconductors surface with self-assembled monolayers (SAMs) has attracted an increased interest in different fields of applications such as biosensors, biomolecular electronics, and gas sensors [9–12]. This can be attributed to their rich and tunable functionalities which can provide a selective binding interaction between these organic receptors and target molecular species [13,14]. The selective sensing using organic/inorganic interfaces was combined with the self-powering capabilities of inorganic heterostructures to produce a selective/self-powered gas sensor as recently reported by Hoffmann et al. [14]. In this study, a self-powered organic/inorganic hybrid sensor (SAM/n-ZnO/p-Si) was fabricated and was capable of selective detection of NO_2 gas (TYPE-2 gas sensor). The resurgent demand for selective detection of nitrogen dioxide is due to its severe impacts on human health and environment [14,15]. Herein, theoretical calculations of work function changes are investigated to understand the effect of different SAMs on the TYPE-2 system. Moreover, the influence of the relative humidity on the response of such organic/inorganic hybrid sensor devices toward NO_2 gas is studied.

This work is comparatively studying these two platforms of self-powered gas sensors and is introducing new insights into their self-powered sensing mechanisms.

EXPERIMENTAL SECTION

Fabrication of TYPE-1 gas sensor. The powering unit of the TYPE-1 sensor is composed of n-ZnO NWs/p-Si substrate junction which have been fabricated according to previously reported procedures [4]. Briefly, a thin film of ZnO (20 nm) was first deposited on Si substrate by DC sputtering using a Zn target (99.99 %) and high purity Ar gas (99.999 %) followed by an annealing in Air at 500 °C for 1 h to produce a crystalline ZnO layer. Vertically aligned ZnO NWs were grown on the ZnO seed layer coated p-Si substrate by using a hydrothermal route at 75 °C for 20 h. The products were washed with deionized water and finally annealed in air at 400 °C for 1 h. The sensing unit (CdS/n-ZnO) is composed by functionalizing the surface of ZnO with CdS nanoparticles (NPs) by using chemical bath deposition; the surface coverage of CdS was controlled by the deposition time. The gas sensing devices were fabricated by using a transparent conductive glass ($F:SnO_2$) as a top contact and the p-side was contacted by silver paste as back electrode [4].

Fabrication of TYPE-2 gas sensor. The powering unit of the TYPE-2 sensor was made of a series of n-ZnO/p-Si diodes as previously reported [14]. By patterning a silicon-on-insulator (SOI) wafer by photolithography, p-Si strips on SiO_2 were prepared. Then, ZnO NWs were site selectively grown by a hydrothermal method (for 3 h at 90 °C) on a ZnO film which was grown by a DC sputtering/thermal annealing method (at 300 °C in air), as mentioned above. The fabricated single diodes were connected in series by evaporating gold contacts using a photolithographic method. The sensing unit is composed of ZnO NWs functionalized with either [3-(2-aminoethylamino)propyl]-trimethoxylsilane or (3-mercaptopropyl)-Trimethoxysilane SAMs.

Fabrication of resistive gas sensor. A resistive gas sensor was fabricated to study the effect of humidity on the sensing unit of TYPE-2 sensor (i.e. organic SAM/ZnO NWs). Briefly, a ZnO film was deposited on interdigitated electrodes (IDEs) made of evaporated gold followed by ZnO NWs growth and finally the devices were functionalized with [3-(2-aminoethylamino)propyl]-trimethoxylsilane by using the same procedure used for fabrication of TYPE-2 sensor.

Gas Sensing measurements. The sensors were placed in a gas sensing chamber with a quartz window for light exposure and gas inlet and outlet. The precise control of gas flow is determined via a flow control system while the sensor signal was recorded by a sourcemeter unit by using a LabView based software (National Instruments Inc.). The sensing measurements were performed under self-powered conditions (i.e. no current applied, under room temperature (23 °C) and under simulated solar illumination).

DFT simulations. The interaction between the thiol and the amine SAM with single NO_2 gas molecules was investigated by Density functional theory (DFT) calculations,

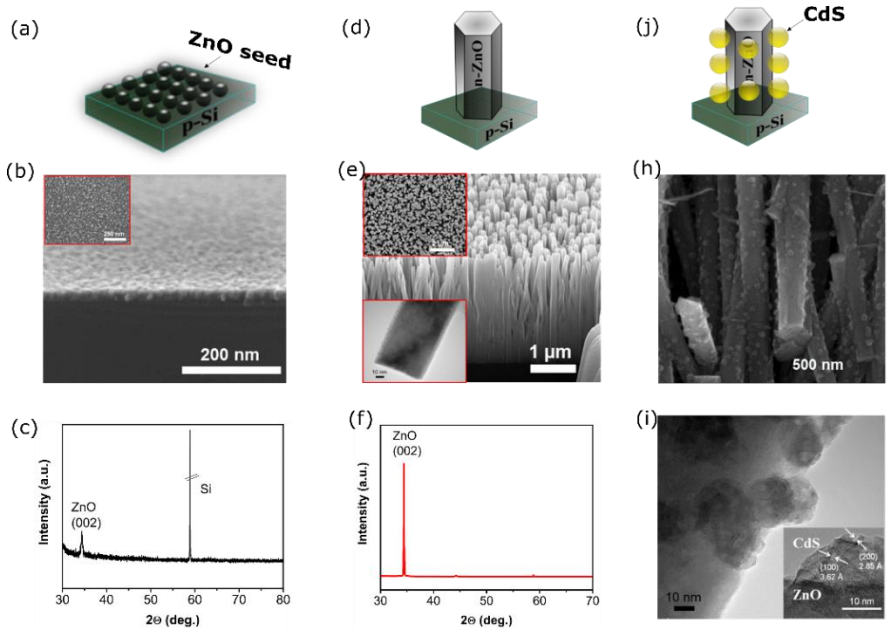

Figure 1. (a-c) Sketch of ZnO seed layer on p-Si substrate, cross-sectional and in plane (inset) SEM image, and the XRD pattern of annealed ZnO seed layer. (d-f) Sketch of ZnO NWs/p-Si substrate, cross-sectional SEM images of ZnO NWs (inset: In plane SEM and TEM images of ZnO NW), and XRD pattern of ZnO NWs. (g-i) Sketch of CdS/ZnO NWs, cross-sectional SEM images, and TEM images (the inset shows the lattice fringes of a CdS NP decorated on the ZnO surface).

which were carried out by using the Vienna Ab initio simulation Package (VASP) [16,17,18]. For the plane wave basis set an energy cut off of 400 eV was employed. A maximal force of 0.01 eV/Å was used as convergence criterium for the ionic relaxations. Since local and semilocal density functionals suffer from the absence of long-range correlation effects [19], the semilocal Perdew-Burke-Ernzerhof functional [20] was combined with Grimme's DFT-D2 correction [21] in order to account for long-range dispersion forces which can be of high importance in the case of otherwise weak chemical interactions.

RESULTS AND DISCUSSION

Self-powered and non-selective gas sensors (TYPE-1 Sensor)

Among the MOx family, ZnO possesses multifunctional merits and it can be synthesized via facile wet chemical routes. The growth of highly oriented and well aligned ZnO NWs directly on their device substrate is crucial for many applications. This can be achieved by using a ZnO seed layer, see Fig. 1a, to promote heterogeneous nucleation and growth of ZnO NWs during the hydrothermal growth. However, the orientation of ZnO NWs is rationally influenced by the crystallinity, orientation, and thickness of the ZnO seed layer [22]. The cross-sectional SEM images of the post-annealed ZnO seed layer show the uniform coating with an average thickness of 20 nm (see Fig 1b, where the inset shows the top-view SEM image of the seed-layer). Figure 1c shows the typical XRD pattern of the post-annealed ZnO seed layer (at 500 °C) deposited on p-Si substrate indicating the enhanced crystallinity with a preferred growth orientation along the (002) plane. Figure 1e shows the SEM top- and cross-sectional view images of the NWs arrays prepared after 20 h growth in a metastable supersaturated solution. ZnO NWs were vertically aligned with uniform size of 150 nm, length of 3 μm and a real density of ~ 20/μm². As shown in Figure 1f, the XRD spectrum of the ZnO arrays shows the strong characteristic diffraction peak (002) of the wurtzite ZnO (JCPDS: 80-0075). It confirms that the as-prepared NW arrays are wurtzite ZnO with vertical orientation along the c-axis.

After fabricating the n-ZnO/p-Si heterojunction (the powering unit), the gas sensing element was realized by uniform assembly of CdS NPs on the ZnO surface as can be seen schematically in Figure 1g~~j~~ and in the cross-sectional SEM images (see Fig. 1h). HR-TEM analysis (Fig. 1i~~j~~) also revealed the homogenous decoration of CdS NPs (diameters, 10-20 nm) on ZnO and the surface of ZnO was not fully covered by CdS. This low coverage density (ca. 11 %) of CdS on ZnO allowed the partially uncovered surface of ZnO to react with gas molecules. HR-TEM image~~s~~ in Figure 1i show also the coherent ZnO-CdS interface. The marked spacing of the crystallographic planes correspond to the (100) and (200) of CdS (see the inset of Figure 1i).

The surface decoration with lower bandgap semiconductors like CdS NPs in the TYPE-1 sensor extends the absorption spectra of the CdS@n-ZnO/p-Si heterostructures to visible light range.

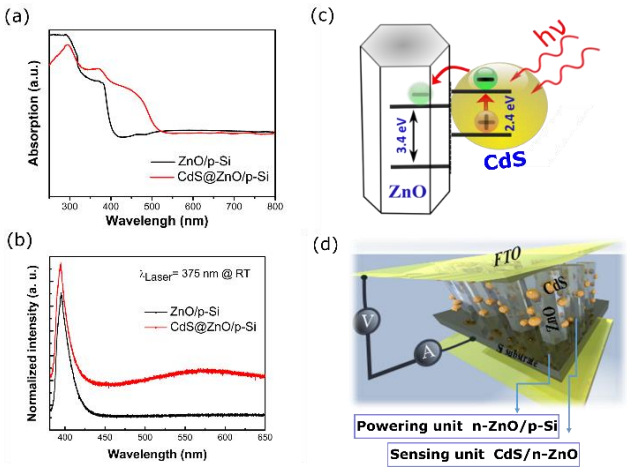

Figure 2. (a) UV-Vis optical absorption spectra of ZnO and CdS@ZnO grown on p-Si substrate. (b) Photoluminescence spectra of ZnO and CdS@n-ZnO systems. (c) Schematic of the band alignment of CdS/ZnO heterostructure. (d) Sketch of the TYPE-1 gas sensing device based on CdS@n-ZnO/p-Si system.

As shown in Fig. 2a, the on-set of optical absorption of CdS@n-ZnO/p-Si sample started from 520 nm whereas the spectrum of naked n-ZnO/p-Si sample is located at 400 nm deriving from the ZnO band gap. Moreover, the photoluminescence (PL) of ZnO and CdS/ZnO systems on p-Si substrate were measured at room temperature with a 375 nm laser diode. Figure 2b exhibits PL spectra of ZnO and CdS-decorated ZnO NWs, where the spectra are dominated by the near band edge emission of ZnO at about 390 nm. The ZnO NWs show a very low defect-related PL peak, however a broad defect luminescence at around 565 nm appears in the CdS@ZnO sample. This broad peak, which is usually assigned to ZnO surface defects in the literature, can be attributed to the surface etching of ZnO during the chemical bath deposition (CBD) of CdS. This effect arises because of the amphoteric nature of ZnO which can be dissolved by the highly basic CBD solution used for the CdS deposition [23]. Additionally, no PL emission related to CdS NPs (with a narrow band gap of 2.4 eV) is observed although the absorption measurement shows an increase of absorbance in the CdS/n-ZnO system. This implies an efficient electron transfer from the CdS NPs to the ZnO NWs which is facilitated by the proper band alignment of the type II heterojunction between CdS and ZnO (see Fig. 2c) [24], whereby the lower conduction band edge of ZnO favors an effective charge separation.

The TYPE-1 device design is shown schematically in Fig. 2d, where the built-in p–n junction is capable of directly harvesting the incident sunlight (simulated sun spectrum; AM1.5, 100 mW/cm^{-2}) and transforming it into an electrical signal which is the open circuit voltage (V_{oc}). Figure 3a shows the dependence of the open circuit voltage changes of CdS@ZnO/p-Si system on the surrounding atmosphere under solar illumination. As can be seen, the open circuit voltage is decreasing upon oxygen exposure, while it is increasing in 1000 ppm ethanol. In other words, the open circuit voltage acts as a self-generated sensor signal that is sensitive and quantitatively correlates to the surrounding gas.

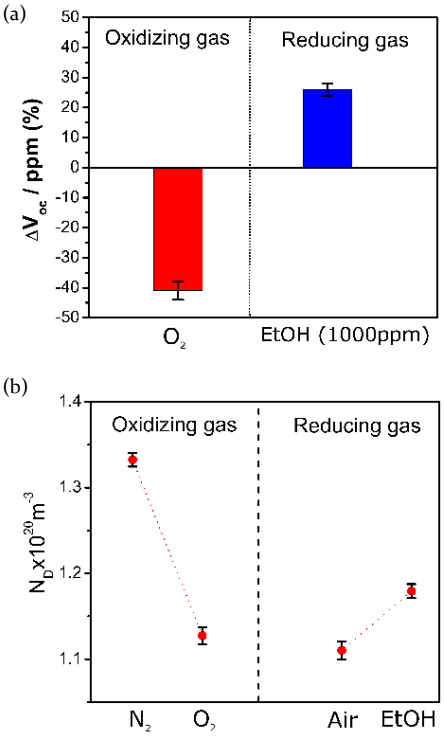

Figure 3. (a) Self-powered sensing responses of TYPE-1 sensor toward oxidizing (O_2) and reducing (1000 ppm ethanol) gases under solar illumination (b) Environmental dependence of N_D of ZnO in the CdS@n-ZnO/p-Si system recorded under solar illumination.

The details of this new sensing mechanism, based on the change of open circuit voltage (ΔV_{oc}), were explained elsewhere [4]. To elucidate the difference of the current sensing mechanism from the well-known conductometric sensing behavior, two experiments were performed with and without applying constant current, respectively. If a constant current is applied to the sensor, the sensing mechanism is the same as for simple conductometric (n-type) gas sensors, in which the resistance increases (i.e. change of resistance, ΔR) with oxidizing gas. This effect can be deduced to the enlargement of the surface depletion zone and it can be monitored by the increase of voltage [25,26]. However, when no current is applied (self-powered mode), the sensing mechanism becomes different since the higher resistance is not influencing the signal. In such case it was found that the change of effective donor density within the n-ZnO material, caused by the interaction with the gas, is arbitrative for the final sensor response. In oxidizing atmospheres, electrons are removed from the n-ZnO and cause a reduction of the effective donor density within the

material. Consequently the build in potential (V_{bi}) [28] of the p-n junction (n-ZnO/p-Si) is reduced and can be monitored by the decrease of open circuit voltage (V_{oc}) or vice versa in case of reducing gases such as ethanol. Figure 3b shows the measured changes of the donor density of CdS@ZnO/p-Si system for different gases [4]. Under dark conditions, the donor density N_D remained constant (ca. 1.20 x 10^{20} m^{-3}), not shown here. Under illumination, the donor density is clearly sensitive to the different gas species (see Figure 3b). The donor density of ZnO was calculated from the slope of $1/C^2$ vs. voltage curve obtained from the capacitance-voltage (C-V) measurements of the CdS@n-ZnO/p-Si NWs heterojunction.

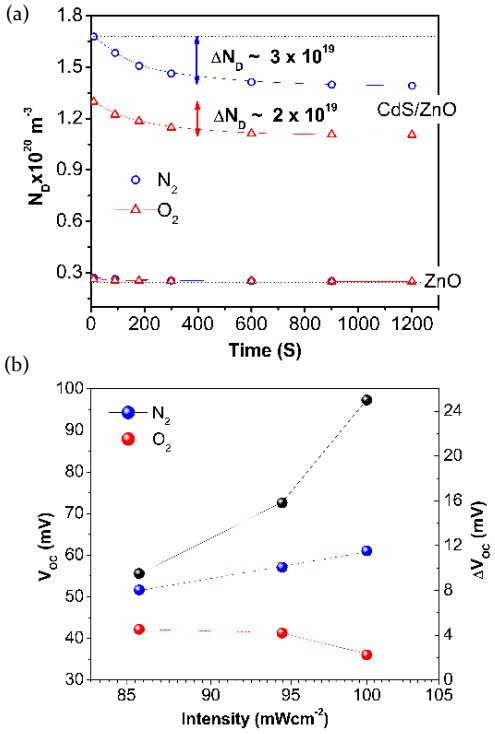

Figure 4. a) Evolution of N_D of CdS@n-ZnO/p-Si and n-ZnO/p-Si devices after switching off the solar light. (b) Light intensity dependence of V_{oc} of CdS@n-ZnO/p-Si system in N_2 and O_2 gases and their relative change (ΔV_{oc}).

To gain a deeper understanding of the sensing mechanism, we studied the dynamic decay behavior of N_D of CdS@n-ZnO/p-Si in comparison to the bare n-ZnO/p-Si systems in order to identify the role of CdS in the sensing mechanism. $1/C^2$ versus applied potential curves for both samples in nitrogen and oxygen atmospheres were measured at different time scales once the solar simulator was switched off (t = 0 s). Figure 4a summarizes the evaluation of N_D at both systems indicating the different N_D changes of CdS@n-ZnO/p-Si and n-ZnO/p-Si systems in N_2 and O_2 atmospheres. The change of donor concentration of bare n-ZnO/p-Si is very small and stabilized at 2.5 x 10^{19} m^{-3} (i.e. insensitive to variation in the gas atmosphere). Whereas, the change of N_D in CdS@n-ZnO/p-Si is more significant (~ 2-3 x 10^{19} m^{-3}) and it is different in N_2 and O_2 atmospheres. It is known that the excited electron (e^{*-}) of CdS is injected into the conduction band of ZnO under illumination. Once the light is switched off, the charge recombination between e^{*-} in ZnO and hole h^+ in CdS will take place. However the interaction between e^{*-} in ZnO and adsorbed oxygen species ($e^{*-} + O_{2\,(g)} \leftrightarrow O_{2\,(ad)}$) will possibly hinder the kinetics of charge recombination in O_2 in comparison to that in N_2 atmosphere and hence these high energy photo-induced electrons will contribute and enhance the sensing response as already observed in the sensing experiments. The here observed behavior is in agreement with the previously depicted sensing mechanism implying the key role of the optical sensitization of CdS/ZnO interface to achieve the sensing response [4].

In classical thermally activated gas sensors, the signal response to gases is modulated by the operation conditions of the sensor due to the temperature dependence of gas adsorption on the sensor surface[27]. Here, the sensing response modulation in relation to the intensity of solar light has been also investigated. Figure 4b shows the relation between incident solar light intensity and the open circuit voltage (V_{oc}), as well as the relative change (ΔV_{oc}) in N_2 and O_2 atmospheres. As shown, the V_{oc} value in N_2 increases linearly with the incident light intensity. In this case, the increase of V_{oc} only depends on the rise of photoelectrons injection from CdS to ZnO and the consequent change in the current, since in principle there is no interaction between ZnO and N_2 (the donor density N_D of ZnO is not modulated by this gas). This situation is very similar to previous reports on CdS/ZnO solar cells, where there is usually a proportional increase of the open circuit voltages with both the light intensity and/or the CdS decoration density [28,29]. On the other hand, in O_2 atmosphere the V_{oc} value drops with higher light intensity values. Due to the increase of injection rate of photoelectrons from CdS to ZnO with higher light intensity, more electrons will react with the oxygen to form the adsorbed oxygen species which will result in a reduction of the effective net donor density in ZnO (N_D) and consequently result in a decrease of V_{oc}. According to the previous assumption, the reduction of donor density of ZnO under oxygen is modulated by the incident light intensity and thus the change of donor density (ΔN_D) is expected to increase (i.e. ΔV_{oc} increases) also with increasing the light intensity. The measured change of open circuit (ΔV_{oc}) values at different light intensities is constituent with the proposed model, and ΔV_{oc} is found to increase with higher light intensities.

To this end, the TYPE-1 gas sensor is a self-powered sensor but it has a non-selective sensing response toward both oxidizing and reducing gases. Therefore, the TYPE-2 sensor is complemented with selective capabilities to overcome the poor selectivity issue. Moreover, the drawbacks of TYPE-1 device design such as long response times and

low open circuit voltage was considered and improved in the TYPE-2 devices.

Self-powered and selective gas sensors (TYPE-2 Sensor)

TYPE-2 self-powered sensor devices, shown schematically in Figure 5a, are based on a similar powering unit used in the TYPE-1 sensor, which here is a nanostructured p-Si/n-ZnO diode that transfers solar light into an electronic signal. The details of the device fabrication process were reported before [14].

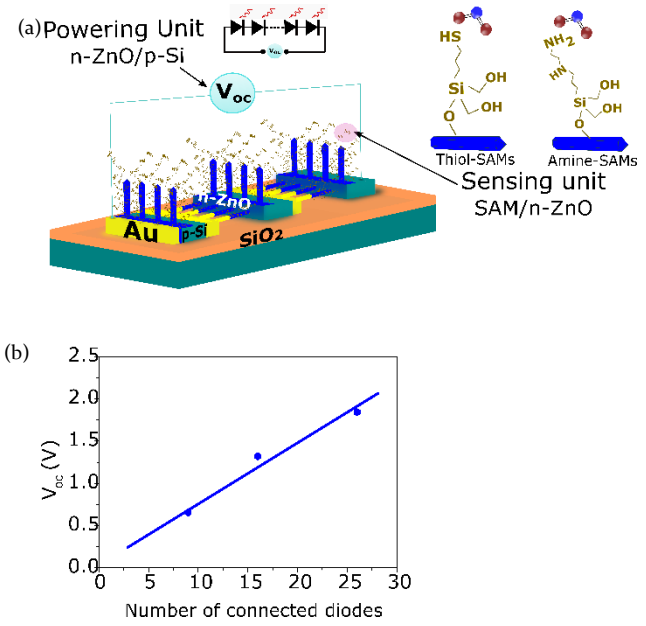

Figure 5. (a) Schematic representation of the TYPE-2 sensor. (b) The linear relation between measured V_{oc} and the number of diodes under illumination (simulated sunlight; AM1.5).

Similar to the TYPE-1 sensor, the produced V_{oc} at the p-n junction serves as a self-generated signal of the gas sensor. However, in order to enhance this self-generated signal and to make it easily measurable in case of low natural light illumination conditions, a number of diode devices were connected in series to increase the measured V_{oc} signal, which is found to be linearly proportional to the number of diodes connected with about 72 ± 6 mV/diode average V_{oc} (see Figure 5b).

After fabricating the powering unit, SAMs are used to construct the sensing element of TYPE-2 sensing devices as reported previously [14]. One of the important advantages of SAMs is that they can couple the external environment to the electronic (current-voltage responses) and the optical properties of their underlying structures [30]. Functionalization of semiconductor surfaces takes place through binding of SAM tail groups to the MOx surface via a condensation reaction such that the exposed terminal functional groups of the SAM can interact with the molecules present in solution or gas phase [14,30]. Figure 5a shows two types of methoxysilane based SAMs that are used for surface modification of ZnO NWs, namely amine ([3-(2-aminoethylamino)propyl]trimethoxylsilane) (amine functionalized-SAM) and thiol ((3-mercapto-propyl)trimethoxysilane) (thiol functionalized-SAM).

The selective response of the amine functionalized and thiol functionalized sensors, respectively, toward NO_2 in comparison to other common interfering gas species such as SO_2, NH_3 and CO (tested at significantly higher concentrations (2.5–25 ppm)) were reported previously [14]. As example, the sensing responses (ΔV_{oc}) toward NO_2 and SO_2 (self-powered mode and under solar light illumination) of the amine functionalized SAM and thiol functionalized SAM are shown in figure 6a. The amine functionalized sensor device selectively detect NO_2 under self-powered operation with an increase of V_{oc} upon exposure to NO_2. On the other hand, the thiol modified ZnO NWs showed a selective negative response toward NO_2 gas with a decrease of V_{oc}. The observed inverted sensor signals for the two sensors with different SAMs functionalities validates the critical role of the gas–SAM surface interactions of the sensor [13,14]. Moreover, the TYPE-2 sensor not only provides a selective gas response in a self-powered operation but also a faster response time compared to TYPE-1 sensors. This can be attributed to the more efficient gas diffusion favored by the open surface provided by the device design of TYPE-2 sensor.

Through investigating the SAM–NO_2 binding geometries and positions of the energy levels of the SAM and the most-stable SAM–NO_2 systems reported elsewhere [13,14], DFT calculations indicated that the lowest unoccupied molecular orbital (LUMO) level of the SAM–gas system for both cases (amine and thiol) is much lower than in the NO_2-free case (see Fig. 6b). Additionally, the relatively low position of the LUMO of thiol–NO_2 and relatively high position of the highest occupied molecular orbital (HOMO) of amine–NO_2 implies a predominantly electron-acceptor character for the first system and a predominantly electron-donor character for the second one which explains the experimentally observed reversed signals between the two functionalized sensors [14]. Furthermore, theoretical calculations revealed a large difference in the surface dipoles induced by amine and thiol functionalized SAMs as shown in Figure 6c,d. In the case of the amine functionalized SAMs, the work function of the system is reduced by 0.9 V with respect to the water terminated MOx surface (see Figure 6c), whereas in the case of the thiol SAMs it is increased by 1.4 V (see Figure 6d). This further confirms that different functionalization – in this case Amine- and Thiol-SAMs – can drastically change the electronic structure of the sensor surface.

However, the effect of such work function changes at the device level is not fully understood at the moment and will be further explored in the future.

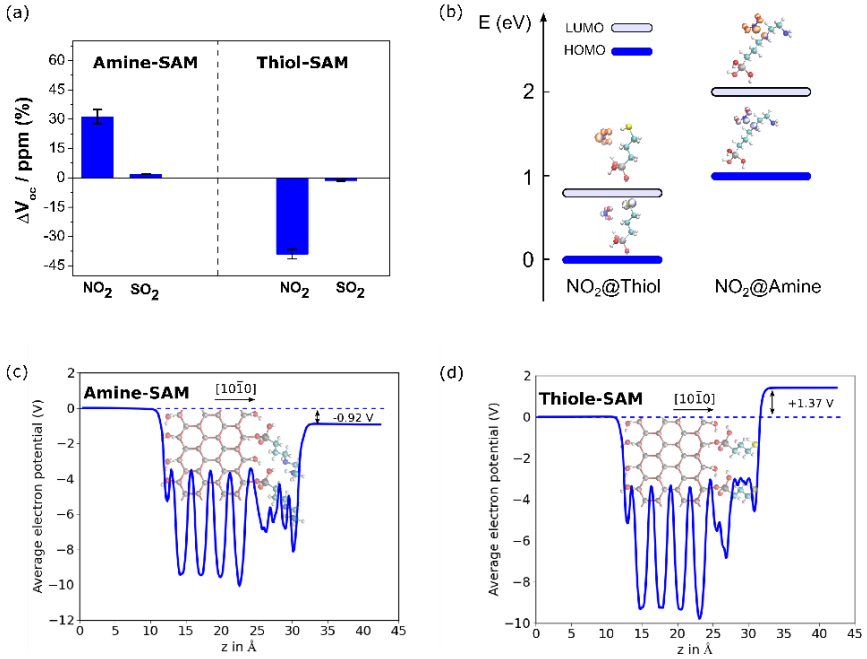

Figure 6. (a) Relative changes of open circuit voltage (Self-powered sensing response) towards NO_2 and SO_2 of amine and thiol functionalized TYPE-2 sensor; (b) Relative alignment of the HOMO and LUMO levels of the amine and thiol functional groups with adsorbed NO2. The adsorption geometries with strongest bonding are shown together with the charge densities of the corresponding HOMO or LUMO level. We mention here that the LUMO levels of the NO2 free functional groups are approximately 3-4 eV higher in energy and thus cannot contribute to charge transfer between SAM and ZnO nanowires; The work function changes of the amine (c) and thiol (d) functionalized SAMs/ZnO systems were calculated from the electron potential averaged in the directions lateral to the surface. The vacuum potential of a (10-10) ZnO surface with an adsorbed monolayer of water.is used as reference and set to zero.

It is worth to mention here that the response toward NO_2 in case of Thiol-SAMs TYPE-2 sensor is constituent with the observed response of the TYPE-1 sensor upon exposure to an oxidizing gas, however, the Amine-SAMs TYPE-2 showed an opposite response towards NO_2, which is different from their response behavior using a resistive sensor approach (Amine/ZnO, see Figure 7). Therefore, on a microscopic level, the development of a comprehensive understanding of the sensing mechanism of such complex system will require additional substantial considerations on a device level in correlation to the surface and interfacial interactions of these sensors. For example, the kinetic and thermodynamic factors of SAM/SAM interactions, their geometrical arrangements, their macroscopic properties (e.g. wetting), and the nature of the MOx surfaces (e.g. surface defects) and the influence of the work function changes on the heterojunction interfaces need further investigations.

The interaction of organic surfaces with humidity is a key issue that can influence their reliable use in real life environmental applications. The effect of relative humidity (R.H.), measured at 23 ºC and 1 atm, on the organic/inorganic hybrid sensor is studied. Here, a traditional conductometric sensor of amine functionalized SAM/ZnO was fabricated for this purpose as a simple model for understanding the effect of humidity on the sensing responses (the change of resistance in this case) and to avoid any complications that can arise from the different interfaces of the p-n junction. As can be seen from Figure 7, the response of the sensor device towards 100 ppb NO_2 gas is changing depending on the amount of relative humidity (R.H.) accompanying the analyte gas. Such enhancement of the sensing response toward analyte gases in presence of R.H. with a faster recovery time were reported before [31] [32] [33]. This indicates a cross sensitivity of the gas sensor toward humidity which might result from the change of the chemical environment due to the adsorbed water at the organic interface. Besides such interfering effect of humidity, the sensor devices showed a good stability against humidity up to 50% (R.H.). ~~however, beyond this R.H. limit the response was affected showing instability.~~ Moreover, above 70% R.H. the sensor signal is unstable and longer measurements lead to its total degradation, which might indicate the degradation of the SAMs on the surface of the sensor. Therefore, more experimental and theoretical investigations are needed to elucidate the humidity interaction mechanisms with the hybrid sensors to enable tailoring their surface properties for a better humidity resistance and minimal interfering with the sensor response.

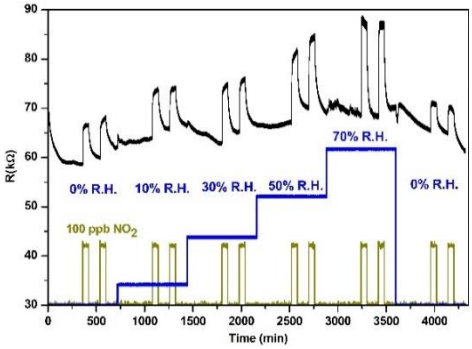

Figure 7. The change of resistance of a conductometric gas sensor based on amine functionalized SAM/ZnO NWs system towards 100 ppb NO_2 with different relative humidity measured at 23 °C and 1 atm.

The general self-powered sensing mechanism:

The term self-powered gas sensors refers to sensing devices that include a built-in powering unit and an active sensing surface in a single heterostructure, where the powering unit is capable of harvesting the energy required for both the sensing signal generating and the surface activation solely from environment. The self-powered sensing mechanism mainly relies on the change of open circuit voltage (ΔV_{oc}) upon interaction with the surrounding ambient. The sensing response can be described by the following steps: firstly a surface interaction with gases and subsequent changes in the metal oxide which is influencing their p-n heterojunction interface and consequently the open circuit voltage (ΔV_{oc}).

For the TYPE-1 sensor (non-selective interaction), ZnO acts as the active sensing surface that interacts with gases via redox interactions causing a change of the effective donor concentration (ΔN_D) of the MOx when enough activation energy is provided. The relation between the donor concentration (N_D) and the built-in potential V_{bi} at the p-n junction interface are expressed by equation 1 [34]:

$$V_{oc}\,\alpha V_{bi} = \frac{KT}{q} ln(\frac{N_D^{ZnO} N_A^{Si}}{N_i^{ZnO} N_i^{Si}}) \qquad [1]$$

where N_D, N_A and N_i are the donor, acceptor and intrinsic doping level, that corresponds to the free carrier concentration in the impurities ionization regime, k, T and q are Boltzmann constant, absolute temperature and electron charge, respectively.

However, for the TYPE-2 sensor, the self-assembled monolayer acts as the active sensing element while ZnO acts as a charge collector. The surface adsorption and the reaction of gas molecules with TYPE-2 sensor result in different band alignment of molecular orbitals of Gas/SAM depending on the type of the SAMs at the organic/inorganic interface. This will result on different donor or acceptor characters of the Gas/SAM and leads to subsequent different changes at the p-n heterojunction interface. The possible scenarios of gas surface interactions with TYPE-1 and TYPE-2 sensors are summarized in Figure8.

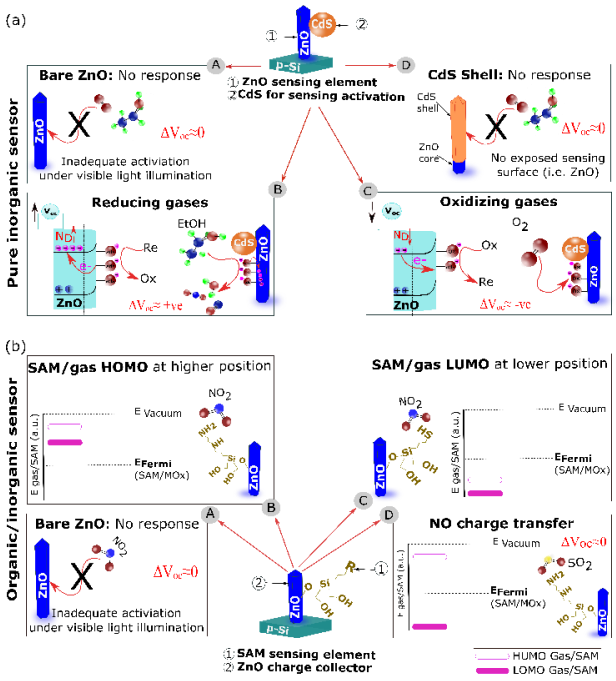

Figure 8. Schematic representations of the possible sensing scenarios in case of (a) TYPE-1 sensor and (b) TYPE-2 sensor.

The self-powered sensing response towards gases can be defined as the (relative) change of open circuit voltage according to equation 2 [14]:

$$\Delta V_{oc}[\%] = \left(\frac{V_{oc}^{gas}}{V_{oc}^{ref}} - 1\right) \times 100 \qquad [2]$$

where $V_{oc,gas}$ is the sensor response in the analyte gas and $V_{oc,ref}$ the sensor response in the reference gas) such as synthetic air).

Conclusions

Two different self-powered gas sensors with either a broad detection range toward oxidizing and reducing gases (based on inorganic heterostructures, TYPE-1 sensor) or with high selectivity towards NO_2 gas (organic/inorganic hybrid structures, TYPE-2 sensor) are comparatively presented here. For both sensors, the (relative) change of open circuit voltage at the p-n heterojunction upon gas exposure act as the self-powered sensing signal. The TYPE-1 sensor is capable of detecting different gases due to the change of the effective donor density of ZnO upon redox interaction with gases. The presence of CdS improves the sensing response through the high energy photo-induced electrons injected at the CdS/ZnO interface. In the TYPE-2 sensor, the surface modification of n-ZnO surface with amine or thiol terminated organic SAMs favored selective sensing of NO_2 gas. Theoretical calculations revealed a large difference in the surface dipoles induced by amine and thiol

functionalized SAMs. This can explain their different sensing behaviors toward NO_2 gas. These two systems combining self-powered operation and gas sensing capabilities (either selective or non-selective sensing) in a singular hetrojunction device opens new avenues for developing miniaturized and maintenance free smart gas sensors.

AUTHOR INFORMATION

Corresponding Authors

***E-mail:** a.gad@tu-braunschweig.de; dprades@el.ub.edu

§ Author Contributions: These authors contributed equally to this manuscript.

The authors declare no competing financial interest.

Acknowledgments

The research leading to these results has received funding from the European Research Council under the European Union's Seventh Framework Programme (FP/2007-2013)/ERC Grant Agreement n. 336917. J.D.Prades acknowledges support from the Serra Húnter Programme. DFT calculations were carried out on the Joe1 cluster at Fraunhofer IWM and on the supercomputer JUROPA at Jülich Supercomputer Centre (JSC). H.Shen is grateful to the BMBF-NanoFutur project (FKZ 03x5512). A.E. Gad and L. Mayrhofer are thankful to the BMBF-WireControl project (FKZ 16ES0292K).

References

(1) Huang, J.; Wan, Q. Gas Sensors Based on Semiconducting Metal Oxide One-Dimensional Nanostructures. *Sensors* **2009**, *9*, 9903–9924.

(2) Monereo, O.; Prades, J. D.; Cirera, A. Self-Heating Effects in Large Arrangements of Randomly Oriented Carbon Nanofibers: Application to Gas Sensors. *Sensors Actuators, B Chem.* **2015**, *211*, 489–497.

(3) Choi, K. J.; Jang, H. W. One-Dimensional Oxide Nanostructures as Gas-Sensing Materials: Review and Issues. *Sensors (Basel).* **2010**, *10*, 4083–4099.

(4) Hoffmann, M. W. G.; Gad, A. E.; Prades, J. D.; Hernandez-Ramirez, F.; Fiz, R.; Shen, H.; Mathur, S. Solar Diode Sensor: Sensing Mechanism and Applications. *Nano Energy* **2013**, *2*, 514–522.

(5) Huber, F.; Riegert, S.; Madel, M.; Thonke, K. H2S Sensing in the Ppb Regime with Zinc Oxide Nanowires. *Sensors Actuators B Chem.* **2017**, *239*, 358–363.

(6) Gad, A. E.; Hoffmann, M.; Leuning, T.; Prades, J. D.; Ramirez, F. H.; Shen, H.; Mathur, S. Solar Driven Zinc Oxide Based Heterojunctions for Gas Sensing Applications. *Conf. Proc. 14th Int. Meet. Chem. Sensors (IMCS 2012)* **2012**, 1312–1315.

(7) Paska, Y.; Stelzner, T.; Christiansen, S.; Haick, H. Enhanced Sensing of Nonpolar Volatile Organic Compounds by Silicon Nanowire Field Effect Transistors. *ACS Nano* **2011**, *5*, 5620–5626.

(8) Wang, B.; Haick, H. Effect of Chain Length on the Sensing of Volatile Organic Compounds by Means of Silicon Nanowires. *ACS Appl. Mater. Interfaces* **2013**, *5*, 5748–5756.

(9) Kobayashi, S.; Nishikawa, T.; Takenobu, T.; Mori, S.; Shimoda, T.; Mitani, T.; Shimotani, H.; Yoshimoto, N.; Ogawa, S.; Iwasa, Y. Control of Carrier Density by Self-Assembled Monolayers in Organic Field-Effect Transistors. *Nat. Mater.* **2004**, *3*, 317–322.

(10) Lessel, M.; Bäumchen, O.; Klos, M.; Hähl, H.; Fetzer, R.; Paulus, M.; Seemann, R.; Jacobs, K. Self-Assembled Silane Monolayers: An Efficient Step-by-Step Recipe for High-Quality, Low Energy Surfaces. *Surf. Interface Anal.* **2015**, *47*, 557–564.

(11) Arya, S. K.; Solanki, P. R.; Datta, M.; Malhotra, B. D. Recent Advances in Self-Assembled Monolayers Based Biomolecular Electronic Devices. *Biosens. Bioelectron.* **2009**, *24*, 2810–2817.

(12) Bhartia, B.; Bacher, N.; Jayaraman, S.; Khatib, S.; Song, J.; Guo, S.; Troadec, C.; Puniredd, S. R.; Srinivasan, M. P.; Haick, H. Application of Organophosphonic Acids by One-Step Supercritical CO 2 on 1D and 2D Semiconductors: Toward Enhanced Electrical and Sensing Performances. *ACS Appl. Mater. Interfaces* **2015**, *7*, 14885–14895.

(13) Hoffmann, M. W. G.; Prades, J. D.; Mayrhofer, L.; Hernandez-Ramirez, F.; Järvi, T. T.; Moseler, M.; Waag, A.; Shen, H. Highly Selective SAM-Nanowire Hybrid NO2 Sensor: Insight into Charge Transfer Dynamics and Alignment of Frontier Molecular Orbitals. *Adv. Funct. Mater.* **2014**, *24*, 595–602.

(14) Hoffmann, M. W. G.; Mayrhofer Dr, L.; Casals Dr, O.; Caccamo, L.; Hernez-Ramirez, F.; Lilienkamp, G.; Daum, W.; Moseler, M.; Waag, A.; Shen, H.; *et al.* A Highly Selective and Self-Powered Gas Sensor via Organic Surface Functionalization of P-Si/n-ZnO Diodes. *Adv. Mater.* **2014**, *26*, 8017–8022.

(15) Zhang, D.; Liu, Z.; Li, C.; Tang, T.; Liu, X.; Han, S.; Lei, B.; Zhou, C. Detection of NO 2 down to Ppb Levels Using Individual and Multiple In 2 O 3 Nanowire Devices. *Nano Lett.* **2004**, *4*, 1919–1924.

(16) Kresse, G.; Furthmüller, J. Efficient Iterative Schemes for Ab Initio Total-Energy Calculations Using a Plane-Wave Basis Set. *Phys. Rev. B* **1996**, *54*, 11169–11186.

(17) Kresse, G.; Joubert, D. From Ultrasoft Pseudopotentials to the Projector Augmented-Wave Method. *Phys. Rev. B* **1999**, *59*, 1758–1775.

(18) Blöchl, P. E. Projector Augmented-Wave Method. *Phys. Rev. B* **1994**, *50*, 17953–17979.

(19) Jones, R. O. Density Functional Theory: Its Origins, Rise to Prominence, and Future. *Rev. Mod. Phys.* **2015**, *87*, 897–923.

(20) Perdew, J. P.; Burke, K.; Ernzerhof, M. Generalized Gradient Approximation Made Simple. *Phys. Rev. Lett.* **1996**, *77*, 3865–3868.

(21) Grimme, S. Semiempirical GGA-Type Density Functional Constructed with a Long-Range Dispersion Correction. *J. Comput. Chem.* **2006**, *27*, 1787–1799.

(22) Yin, Y. T.; Que, W. X.; Kam, C. H. ZnO Nanorods on ZnO Seed Layer Derived by Sol–gel Process. *J. Sol-Gel Sci. Technol.* **2010**, *53*, 605–612.

(23) Panigrahi, S.; Basak, D. Morphology Driven Ultraviolet Photosensitivity in ZnO-CdS Composite. *J. Colloid Interface Sci.* **2011**, *364*, 10–17.

(24) Nayak, J.; Sahu, S.; Kasuya, J.; Nozaki, S. CdS–ZnO Composite Nanorods: Synthesis, Characterization and Application for Photocatalytic Degradation of 3,4-Dihydroxy Benzoic Acid. *Appl. Surf. Sci.* **2008**, *254*, 7215–7218.

(25) Gad, A. E.; Hoffmann, M. W. G.; Hernandez-Ramirez, F.; Prades, J. D.; Shen, H.; Mathur, S. Coaxial P-Si/n-ZnO Nanowire Heterostructures for Energy and Sensing Applications. *Mater. Chem. Phys.* **2012**, *135*, 618–622.

(26) Wang, C.; Yin, L.; Zhang, L.; Xiang, D.; Gao, R. Metal Oxide Gas Sensors: Sensitivity and Influencing Factors. *Sensors* **2010**, *10*, 2088–2106.

(27) Oberhüttinger, C.; Hackner, A.; Müller, G.; Stutzmann, M. On the Temperature Dependence of the Resistive and Surface Ionisation Response of SnO2 Gas Sensing Layers. *Sensors Actuators B Chem.* **2011**, *156*, 563–571.
(28) Tak, Y.; Hong, S. J.; Lee, J. S.; Yong, K. Fabrication of ZnO/CdS Core/shell Nanowire Arrays for Efficient Solar Energy Conversion. *J. Mater. Chem.* **2009**, *19*, 5945.
(29) Zhang, Y.; Xie, T.; Jiang, T.; Wei, X.; Pang, S.; Wang, X.; Wang, D. Surface Photovoltage Characterization of a ZnO Nanowire array/CdS Quantum Dot Heterogeneous Film and Its Application for Photovoltaic Devices. *Nanotechnology* **2009**, *20*, 155707.
(30) Love, J. C.; Estroff, L. a; Kriebel, J. K.; Nuzzo, R. G.; Whitesides, G. M. Self-Assembled Monolayers of Thiolates on Metals as a Form of Nanotechnology. *Chem. Rev.* **2005**, *105*, 1103–1170.
(31) Beer, S.; Helwig, A.; Müller, G.; Garrido, J.; Stutzmann, M. Water Adsorbate Mediated Accumulation Gas Sensing at Hydrogenated Diamond Surfaces. *Sensors Actuators B Chem.* **2013**, *181*, 894–903.
(32) Maier, K.; Helwig, A.; Müller, G.; Hille, P.; Eickhoff, M. Effect of Water Vapor and Surface Morphology on the Low Temperature Response of Metal Oxide Semiconductor Gas Sensors. *Materials (Basel).* **2015**, *8*, 6570–6588.
(33) Offermans, P.; Vitushinsky, R. <formula Formulatype="inline"><tex Notation="TeX">${\rm NO}_{2}$</tex></formula> Detection With AlGaN/GaN 2DEG Channels for Air Quality Monitoring. *IEEE Sens. J.* **2013**, *13*, 2823–2827.
(34) Sze, S.; Ng, K. *Physics of Semiconductor Devices*; (John Wiley & Sons, New Jersey, 2007), 2006.

For TOC only

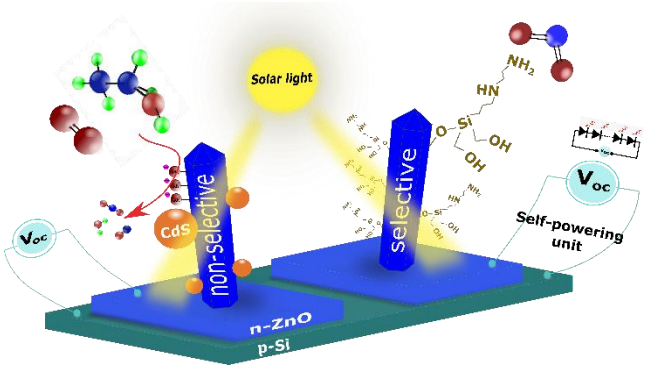
Solar light
non-selective
selective
CdS
n-ZnO
p-Si
Voc
Voc
Self-powering unit
NH2
HN
Si
OH
OH